Available online at www.sciencedirect.com

ScienceDirect

Publishing Services by Elsevier

International Journal of Naval Architecture and Ocean Engineering 9 (2017) 382–389

http://www.journals.elsevier.com/international-journal-of-naval-architecture-and-ocean-engineering/

# Effect of wing form on the hydrodynamic characteristics and dynamic stability of an underwater glider

Muhammad Yasar Javaid [a,*], Mark Ovinis [a,**], Fakhruldin B.M. Hashim [a], Adi Maimun [b], Yasser M. Ahmed [b,c], Barkat Ullah [a]

[a] Department of Mechanical Engineering, Universiti Teknologi PETRONAS, Perak, Malaysia

[b] Marine Technology Centre, Faculty of Mechanical Engineering, Universiti Teknologi Malaysia, Johor Bahru, Malaysia

[c] Dept. of Naval Architecture and Marine Engineering, Faculty of Engineering, Alexandria University, Alexandria, Egypt

Received 25 May 2016; revised 16 September 2016; accepted 25 September 2016

Available online 25 October 2016

**Abstract**

We are developing a prototype underwater glider for subsea payload delivery. The idea is to use a glider to deliver payloads for subsea installations. In this type of application, the hydrodynamic forces and dynamic stability of the glider is of particular importance, as it has implications on the glider's endurance and operation. In this work, the effect of two different wing forms, rectangular and tapered, on the hydrodynamic characteristics and dynamic stability of the glider were investigated, to determine the optimal wing form. To determine the hydrodynamic characteristics, tow tank resistance tests were carried out using a model fitted alternately with a rectangular wing and tapered wing. Steady-state CFD analysis was conducted using the hydrodynamic coefficients obtained from the tests, to obtain the lift, drag and hydrodynamic derivatives at different angular velocities. The results show that the rectangular wing provides larger lift forces but with a reduced stability envelope. Conversely, the tapered wing exhibits lower lift force but improved dynamic stability.



*Keywords:* Underwater glider; Hydrodynamic characteristics; Dynamic stability

## 1. Introduction

An Underwater Glider (UG) is a self-propelled unmanned underwater vehicle with wings that convert vertical motion into horizontal motion. The wing form of these gliders influenced their hydrodynamic characteristics. The hydrodynamic characteristics may be obtained experimentally or numerically. Experimental studies are expensive and tedious, as it entails among others, availability of test facilities, fabrication of a prototype, calibration, experimental setup, etc. On the other hand, numerical simulation does not have these drawbacks and is a proven alternative to experimental studies. Nevertheless, an effective model, appropriate boundary conditions and selection of correct mesh size are needed to achieve good results (Stern et al., 2013). The hydrodynamic forces and moments acting on the glider in turn affect its dynamic stability. Stability is important, as the glider's external control surfaces such as its wings typically operate in a low-speed environment, and as such are unable to make quick corrective actions.

Zhang et al. (2014) evaluated the lift to drag ratio of a fish-like robot with a simple non-standard trapezoidal wing at different wing aspect ratio. They found that larger wings result in shallower gliding paths i.e. longer horizontal travel, but slower total speed compared to smaller wings. Liu et al. (2014) investigated the effect of wing layout on the maneuverability of a hybrid underwater vehicle Petrel-II, specifically the influence of chord length, aspect ratio, sweep back angle and axial position. They found that chord length has a

* Corresponding author. Fax: +60 5 365 6461.

** Corresponding author. Fax: +60 5 365 6461.

*E-mail addresses:* yasar248@gmail.com (M.Y. Javaid), mark_ovinis@petronas.com.my (M. Ovinis).

Peer review under responsibility of Society of Naval Architects of Korea.

http://dx.doi.org/10.1016/j.ijnaoe.2016.09.010

significant impact on the lift to drag ratio, while sweep angle has a significant impact on the movement of the vehicle. In this work, we investigated the effect of wing form on the lift to drag ratio and stability, by replicating both a straight-line resistance test and a rotating arm test using Computational Fluid Dynamics (CFD) in three dimensions.

The layout and dimensions of the newly developed glider, the UTP glider, are provided in Fig. 1 and Table 1, respectively. The glider consists of an elliptical hull and vertical rudder, with an interchangeable tapered and rectangular wing. Both wings have a NACA 0016 airfoil shape. The lift, drag, pitching moment, rotating arm normal forces and pitching moment of the glider with both the rectangular and tapered wing were compared. Additionally, the dynamic stability of both wing forms was evaluated analytically.

In Section Two, a dynamic model of the UTP glider along the vertical plane and its corresponding dynamic stability equations are described. Section Three describes the detailed CFD simulation methodology. In the last section, we present and discuss the results of the straight-line resistance test and rotating arm test for the UTP glider with rectangular and tapered wings.

## 2. Dynamic equations of motion

The motion of the UTP glider is based on the six Degrees of Freedom (DOF) body fixed coordinate, the origin of which is the Center of Buoyancy (CB), as shown in Fig. 2. Table 2 lists the respective motion parameters and the corresponding axes in the body fixed coordinate system.

In general, the dynamic behavior of an underwater glider is highly complex due to nonlinear coupling of forces and moments in 6-DOF. The 6-DOF equations of motion of the glider were simplified along the horizontal and vertical plane, with the assumption that the forces and moments are functions of velocity and acceleration. The linearized model of the glider in the vertical plane (Fossen, 2011) are expressed as follows:

$$-X_u U + (m - X_{\dot{u}})\dot{U} = 0 \tag{1}$$

$$(m - Z_{\dot{w}})\dot{w} - Z_w w - (mx_G - Z_{\dot{q}})\dot{q} - (mU + Z_q)q = 0 \tag{2}$$

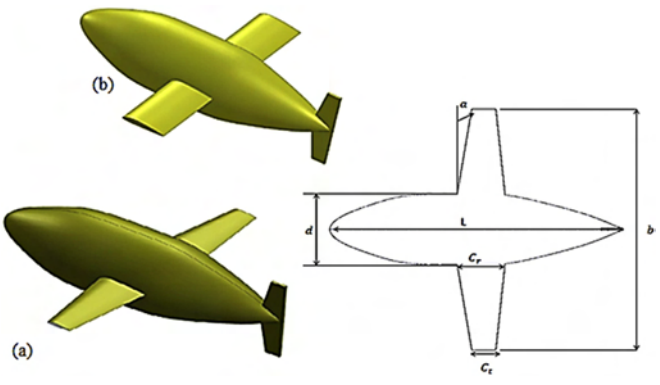


Fig. 1. Underwater glider with (a) tapered wings (b) rectangular.

$$-(mx_G + M_{\dot{w}})\dot{w} + (I_{yy} - M_{\dot{q}})\dot{q} - M_w w + (mx_G U - M_q)q = 0 \tag{3}$$

### 2.1. Dynamic stability

Vertical and horizontal stability are important to ensure good path stability and turning performance. A highly maneuverable glider requires dynamic stabilities in both horizontal and vertical directions. While a stable glider without any control input may have straight line stability in the horizontal plane, hydrostatic restoring forces and moments are prone to destabilize the glider in the vertical plane. The stability of a glider is controlled by a moving internal mass or. Alternatively, the dynamic stability of a glider may be controlled by external fixed wings and a vertical rudder. The Routh stability criteria for dynamic stability in heave and pitch are given in Eqs. (4) and (5).

$$Z_w M_q - M_w(y_r + mw) > 0 \tag{4}$$

$$\frac{Z_w}{(Z_q + mw)} - \frac{M_w}{M_q} > 0 \tag{5}$$

Table 1
UTP glider dimension.

| Dimension | Rectangular wings glider | Taper wings glider |
|---|---|---|
| Total wing span (b) | 0.97 m | 0.97 m |
| Root chord length $C_r$ | 0.17 m | 0.17 m |
| Glider diameter d | 0.28 m | 0.28 m |
| Glider length (L) | 1.04 m | 1.04 m |
| Taper ratio $C_r/C_t$ | – | 1.89 |
| Sweep angle (a) | – | 8.5° |

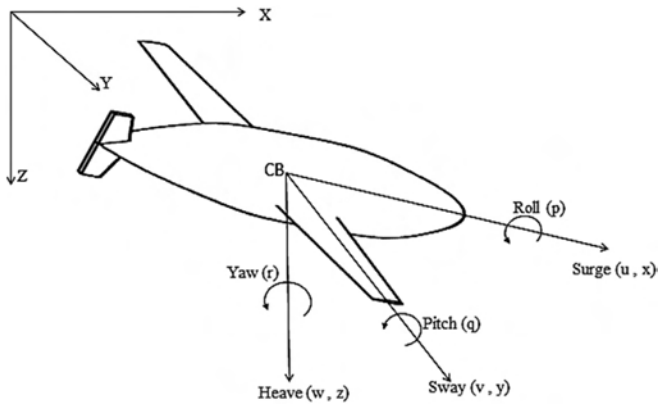


Fig. 2. Glider body fixed coordinate system.

Table 2
Motion parameters and their corresponding axes.

| DOF | Displacement | Force & Moment | Velocity | Acceleration |
|---|---|---|---|---|
| 1-surge | x | X | u | $\dot{u}$ |
| 2-sway | y | Y | v | $\dot{v}$ |
| 3-heave | z | Z | w | $\dot{w}$ |
| 4-roll | $\phi$ | K | p | $\dot{p}$ |
| 5-pitch | $\theta$ | M | q | $\dot{q}$ |
| 6-yaw | $\psi$ | N | r | $\dot{r}$ |

In Eq. (5), the first term represents the ratio of force in the vertical plane and the second term represents the moment force. For a stable glider, the moment of a dynamic body must be greater than its linear velocity. Stability along the vertical plane, $G_V$ is given by;

$$G_V = 1 - \frac{M_w(Z_q + mv)}{M_q Z_w} \tag{6}$$

Similarly, the stability equation along the horizontal plane is written as;

$$G_H = 1 - \frac{N_v(y_r - mv)}{N_r y_v}$$

A non-zero dynamic stability margin indicates unstable motion (Phillips, 2010).

### 2.2. Glider performance

The performance of a glider i.e. its glide ratio, horizontal velocity and sink rate, are closely related to its hydrodynamic characteristics. Moreover, the operational velocity of the glider is analogous to the buoyancy change across the ocean. Lung capacity factor$\overline{\eta}$ is represented as a ratio of the maximum displaced volume, $V_{vol}$ and the neutral buoyancy volume, $V_{NB}$ minus 1.

$$V_{vol} = (1 + \overline{\eta})V_{NB} \Leftrightarrow \overline{\eta} = \frac{V_{vol}}{V_{NB}} - 1 \tag{7}$$

The total dry weight of glider 'W' at neutral buoyancy is $W = \rho g V_{NB}$, the net weight of glider '$\overline{W}$' is

$$\overline{W} = W - B$$

$$\overline{W} = \rho g V_{NB} - \rho g(1 + \eta)V_{NB}$$

$$\overline{W} = -\rho g \eta V_{NB} = -\frac{\eta}{1 + \overline{\eta}} \rho g V_{vol} \tag{8}$$

Graver (Graver, 2005) described the steady state dynamic equation of an underwater glider as follows:

$$V = \sqrt{\frac{\overline{w}\cos(\gamma)}{K_{L0} + K_L \alpha}} \tag{9}$$

where, $K_{LO}, K_L$ is lift force coefficients

V velocity of glider
$\alpha$ Angle of attack
$\gamma$ Glide angle
$\overline{w}$ Net buoyancy force

The relationship between the optimal angle of attack and glide angle with hydrodynamic coefficients from Eqs. (4)–(6) (Graver, 2005) is given by Equation (10) below:

$$\alpha = \frac{1}{2K_D}\left( - K_L \tan(\theta) - \sqrt{(K_L \tan(\theta))^2 - 4K_D(K_D \tan(\theta) + K_{D0})} \right) \tag{10}$$

## 3. Methodology

Steady-state CFD analysis were performed to determine the hydrodynamic characteristics and dynamic stability of the glider. The motion of the fluid is modeled using ANSYS FLUENT 16 based on the incompressible (Eq. (11)) Reynolds Averaged Navier Stokes (RANS) equation (Eq. (12)) to determine the flow field and pressure around the glider hull.

$$\text{Continuity} : \frac{\partial U_j}{\partial x_j} = 0 \tag{11}$$

$$\rho \frac{\partial \overline{U_i}}{\partial t} + \rho \frac{\partial \overline{U_j U_i}}{\partial x_j} = -\frac{\partial \overline{P}}{\partial x_i} + \frac{\partial}{\partial x_j}\left( \mu \left( \frac{\partial \overline{U_i}}{\partial x_j} + \frac{\partial \overline{U_j}}{\partial x_i} \right) \right) - \rho \frac{\partial \overline{U_j' U_i'}}{\partial x_j} + \overline{F_i} \tag{12}$$

where, $\rho \frac{\partial u_j u_i}{\partial x_j}$ is convection term of Reynolds decomposition, $\rho \frac{\partial \overline{U_j U_i}}{\partial x_j}$ represent leads terms and $\rho \frac{\partial \overline{U_j' U_i'}}{\partial x_j}$ extra terms denote as Reynolds stress tensor. Currently, different turbulence models are employed to solve the Reynolds stress tensor to determine the unknown values. Jagadeesh et al. (2009) recommends a low Reynolds turbulence model for investigation of autonomous underwater vehicles because the Reynolds number range between $1 \times 10^5$ to $1 \times 10^6$ for these vehicles, which are typically designed for low speeds of between 0.25 m/s to 0.5 m/s (Zhang et al., 2013). The K−$\epsilon$ turbulence model, which effectively describes the fluid behavior in the above-mentioned range of Reynolds number, was selected for this study.

### 3.1. Computational domain

The fluid domain is based on the ITTC (Bertram, 2011) guidelines, which recommends that the upstream boundary should be 1–2 times the length of the glider, $L_{glider}$ and the downstream boundary should be 3–5 times $L_{glider}$, to avoid any blockages by the walls. Similar work (Zhang et al., 2013; Javaid et al., 2015) on submerged bodies concluded that the inlet position should be 1.5 times $L_{glider}$ away from the body and the outlet must be 3.5 times $L_{glider}$. The top, bottom and side wall shall be kept 9 times the diameter of the glider, $D_{glider}$ to avoid the interruption in fluid flow (Zhang et al., 2013; Javaid et al., 2015). The fluid domain consists of a flow velocity inlet, pressure outlet, ceiling, bottom wall, and two sidewalls. A domain independency test was conducted with different inlet, outlet and sidewall position with fine mesh using RNG k-$\epsilon$ model at zero drift angle using Froude number,

Fr of 0.33. The test suggested an optimal domain size of $2L_{inlet} \times 4L_{outlet} \times 8D_{side\text{-}wall}$, as shown in Fig. 3.

Rotating arm: A fluid domain, as shown in Fig. 4, was generated to replicate a rotating arm test, to simulate the rotary motion of the glider. The flow inlet velocity was varied to achieve the required circumferential velocity at a constant radius, R of 13 m. The angular velocity of the flow 'q' is given by Equation (13),

$$q = \frac{V}{R} \tag{13}$$

### 3.2. Grid generation

The fine unstructured mesh was generated automatically, using the CFD Fluent functionality in Ansys workbench. The number of mesh were set to $4 \times 10^6$ to $4.6 \times 10^6$, based on the grid independence of the mesh, as shown in Figs. 5 and 6

## 4. Results and discussion

### 4.1. Tow tank test

In order to validate the CFD simulation results, a series of tow tank experiments for a glider with a NACA0016 airfoil tapered wing were conducted at the Marine Technology Center, Universiti Teknologi Malaysia. Fig. 7 shows the tow tank setup, with the UTP glider fixed with to a carriage. The prototype glider was fixed to carriage through struts to maintain the free surface distance of 3D (D = diameter) of glider. An aero-foil shield was used to cover the struts to minimize the drag due to the struts. The drag force of the entire setup without the glider was first determined, and this was subsequently subtracted from the total drag force of the setup including glider, to obtain the drag force on the glider itself.

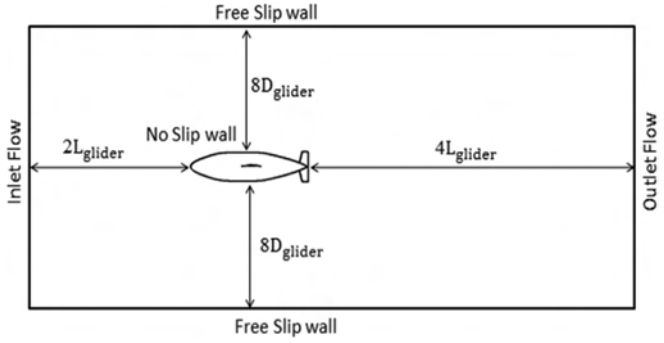


Fig. 3. Fluid domain for straight-line simulation.

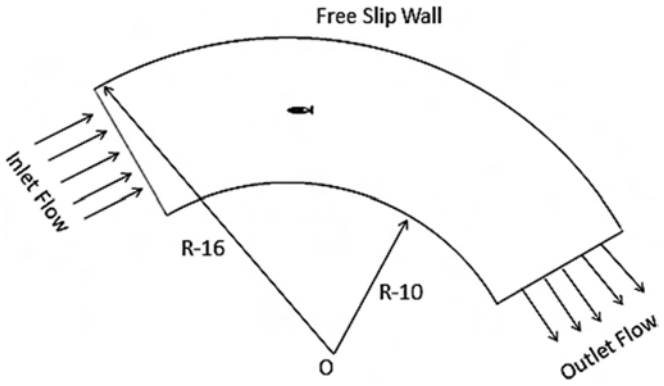


Fig. 4. Fluid domain for rotating arm simulation.

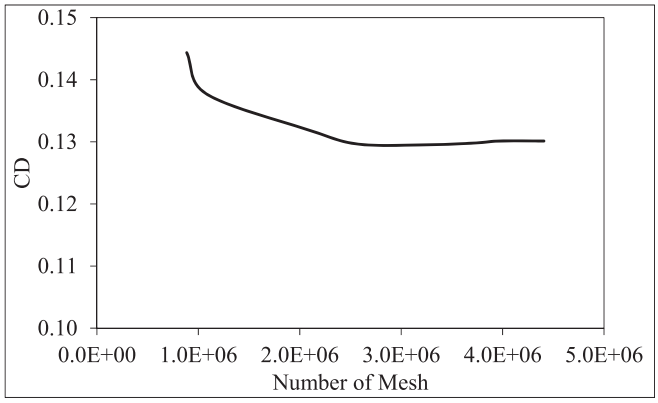


Fig. 5. Grid independency for drag coefficient, $C_D$.

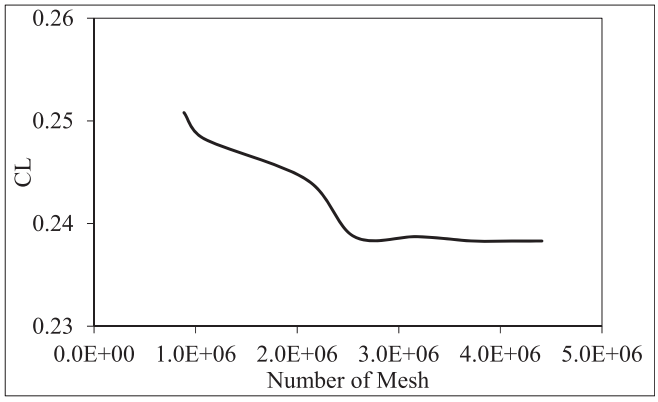


Fig. 6. Grid independency for lift coefficient, $C_L$.

### 4.2. Drag force ($F_D$)

Table 3 and Fig. 8 are shows the experimental and simulation results for the drag force on the tapered wing glider. Generally, the simulation results shown are in good agreement with experimental results, with a maximum error of 6.9%. It is believed that the disagreements in the experimental and numerical calculations are due to the different conditions of both tests. In the tow tank straight-line resistance test, the model was towed with a carriage, while for the simulation; flow was created around the glider model. Additionally, discrepancies may be due to the variation of carriage speed or flow vortices during experiment. Similarly, discrepancies may be due to imperfect selection of flow model, number of inflation layers, selection of fluid domain etc. for the simulation.

The magnitude of the drag force slightly increases with an increase in the Froude number (Fr). This is because of a pressure drop around the glider body with an increase in Fr,

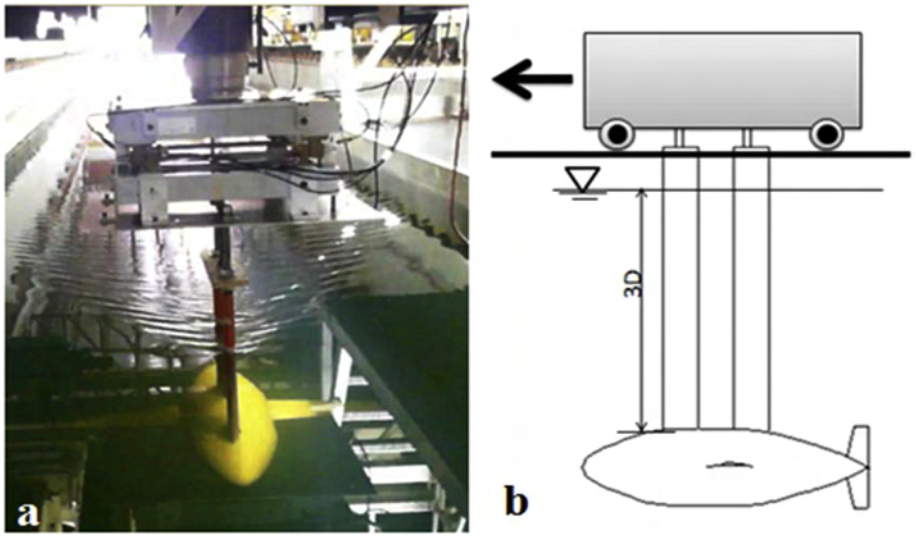


Fig. 7. Tow tank test and schematic of the test.

Table 3
Drag force at various Froude numbers.

| Fr | CFD | Experimental | Error |
|---|---|---|---|
| 0.33 | 0.577494 | 0.563013 | 2.50 |
| 0.55 | 1.393193 | 1.315216 | 5.59 |
| 0.77 | 2.617866 | 2.471175 | 5.60 |
| 1.10 | 4.962295 | 5.305635 | 6.91 |

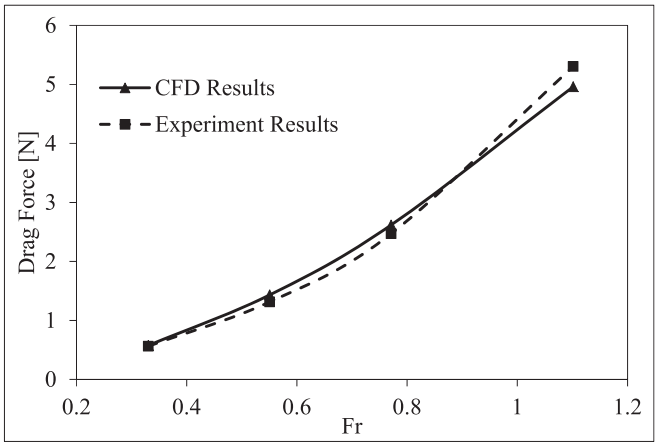


Fig. 8. Variation of drag force with Froude number.

which compresses the boundary layer, resulting in higher friction and viscosity.

### 4.3. Lift force ($F_L$)

The normal component of the resultant force during the movement of a glider is called lift force. Lift force acts normal to the flow direction and opposite to gravitational force. The lift force acting on a glider is a function of fluid density, the velocity of the fluid and the shape of the glider at zero drift angles. It is a positive function of Froude number (Fr). Large amounts of lift force are attributed to a pressure drop due to flow separation between the nose and tail of a glider. Hence, this negative pressure leads to a huge amount of lift force. Fig. 9 is shown that the numerical and experimental values for the lift force.

### 4.4. Comparison of rectangular and tapered wings

Fig. 10 shows a comparison of the drag force at various pitch angles for the glider with a rectangular and tapered wing form at Fr between 0.33 and 1.10. There is a considerable increase in the drag and lift forces of the rectangular wing, as compared to tapered wings. This can be explained by referring to the difference in wetted surface between the two, because drag force acts on the horizontal plane opposite to the resistance force of the glider and is a function of the wetted surface. The increase in drag force of the rectangular wing is calculated by the following equation.

$$\text{Increment } (\%) = \frac{F_{D(\text{Rectangular})}}{F_{D(\text{Tapered})}} - 1$$

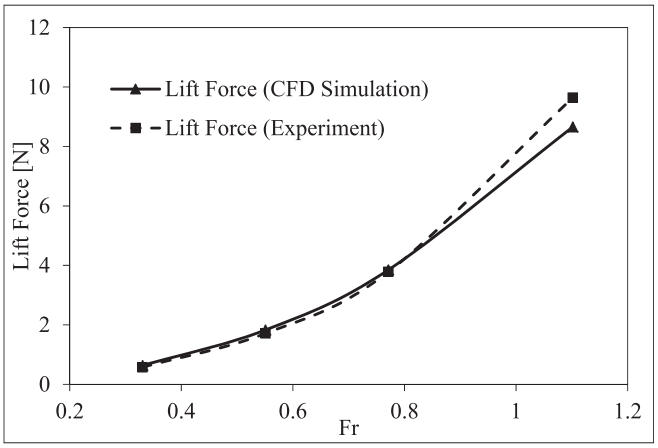


Fig. 9. Variation of lift force with Froude number at zero degree of drift angle.

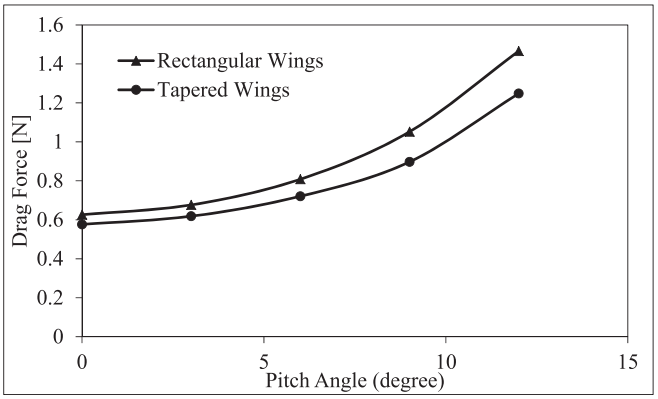


Fig. 10. Variation of drag force with pitch angle.

The drag force of a glider with rectangular wings is 15% higher relative to a glider with tapered wings at a pitch angle of 12°. The difference in drag force is large because wetted surface or blockage area of the rectangular wing form at pitch angle of 12° is greatest.

Fig. 11 shows the variation of lift force with pitch angle at Fr = 0.33. The increment in lift force of the glider with rectangular wing is calculated using the following equation.

$$\text{Increment } (\%) = \frac{F_{L(\text{Rectangular})}}{F_{L(\text{Tapered})}} - 1$$

Lift force is dependent on the interaction of a surface with the flow field. With an increase in the angle of attack, more surface area interacts with the flow field, generating more lift force. However, the lift force decreases beyond the critical pitch angle. At the critical angle of attack, the flow separates from the upper surface of the body and generates less deflection in the downward direction. Hence, the resulting lift force decreases. The glider with the rectangular wing has 6% more lift force at the critical pitch angle of 9° but considerably 17% more lift at pitch angle of 12°. This is because flow separation is highly dominant beyond the critical angle of attack, generating low lift force and high drag force, as shown in Fig. 12.

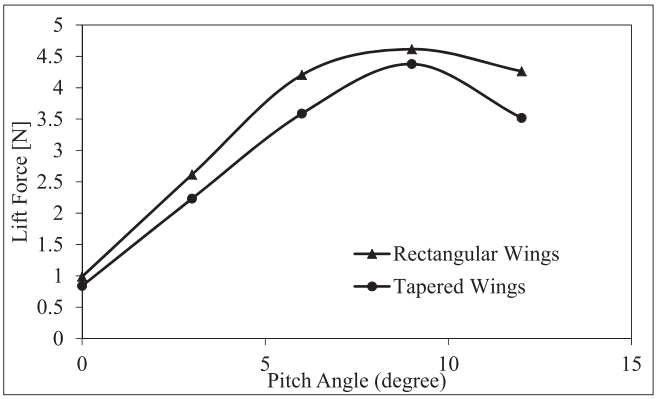


Fig. 11. Variation of lift force with pitch angle.

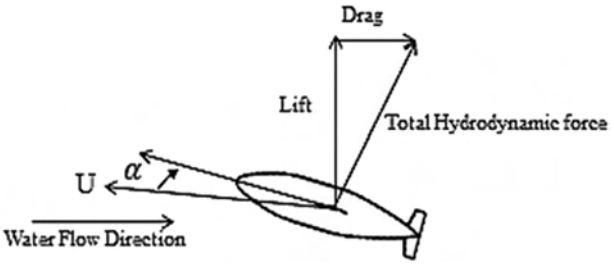


Fig. 12. Variation of lift and drag force with angle of attack.

### 4.5. Drag polar

The relationship between lift force and drag force is denoted by a drag polar curve (Bertin and Smith, 1998). Fig. 13 shows that the average drag polar curve for a glider with rectangular wings is higher as compared to a glider with tapered wings. The difference between a glider with rectangular and tapered wings is more pronounced beyond critical angle of attack. The highest lift to drag ratio is at an angle of attack of around 16%, as the rectangular wing has a larger wetted surface area as compared to tapered wings.

### 4.6. Glide performance

Fig. 14 shows the horizontal velocity at various glide angle of the UTP glider for both wing forms, for different lung capacity factors. The maximum velocity of glider was observed at 33° glide angle. It is noted that the velocity of a glider with tapered wings was 16% higher at 33° glide angle when compared with a glider with rectangular wings. The glider with tapered wing has a speed advantage over a glider with rectangular wings, because of less drag. However, the velocity increases up to 55% with an increment of lung capacity factor from 0.02 to 0.05 for both wing forms.

### 4.7. Stable glider performance

Dynamic motion stability and maneuverability is an important factor to define at the early stage of design for any

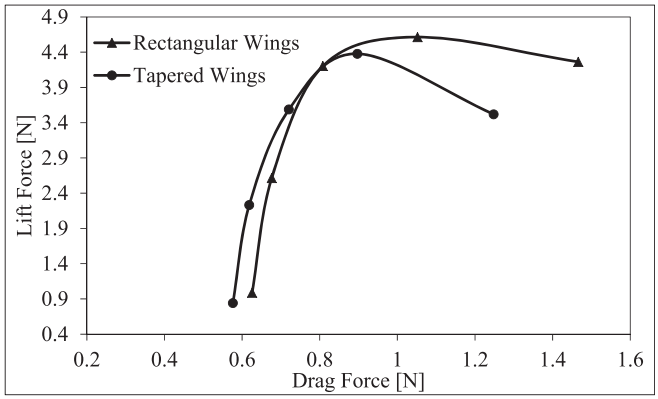


Fig. 13. Lift to drag coefficient (lift-drag polar curve).

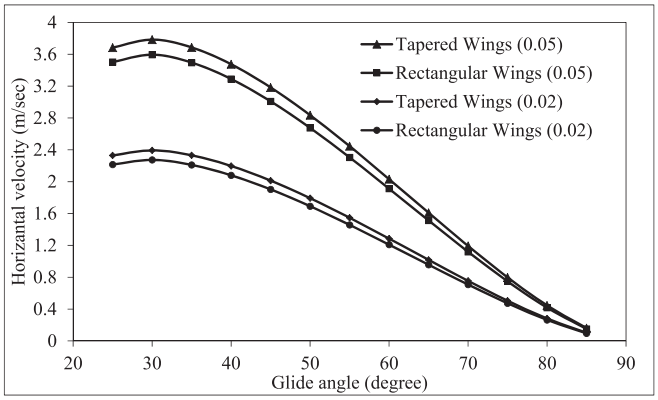


Fig. 14. Variation of horizontal speed and glide angle.

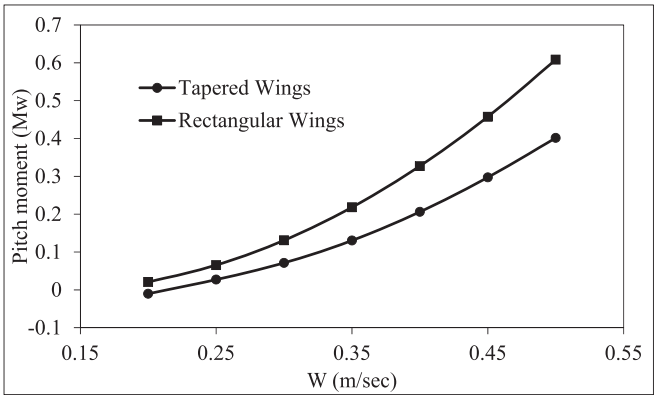


Fig. 17. Variation of pitch moment ($M_w$) and pitch velocity (W).

underwater vehicles. The dynamic stability, hydrodynamic forces and moments were determined using a straight-line test and rotary arm test.

*4.7.1. Straight-line test*

This test is similar a tow tank resistance test. In this test, the normal force (heave force) along the direction of z-axis and corresponding pitch moment (M), as shown in Fig. 15 can be determined. The coefficients along the heave force and moment were determined from the gradient of the heave velocity and pitch moments plots, as shown in Figs. 16 and 17.

Fig. 16 illustrates the variation of the normal force with velocity for a tapered and rectangular wing glider. The glider with rectangular wings has a 15% higher normal heave force as compared to a glider with tapered wings. This is because the large area between leading edge to tail edge creates higher normal force acting at the wings. The pitch force, $M_w$ are determined from the slope of the pitch moment, M with velocity as shown in Fig. 17. The rectangular wings glider showed higher pitching moment as compared to tapered wings glider which can be fixed through normal force for stable glide path (Javaid et al., 2015).

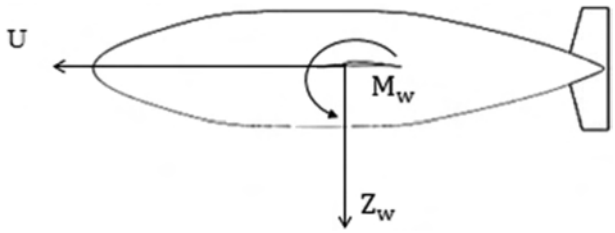


Fig. 15. Force and moment components of glider.

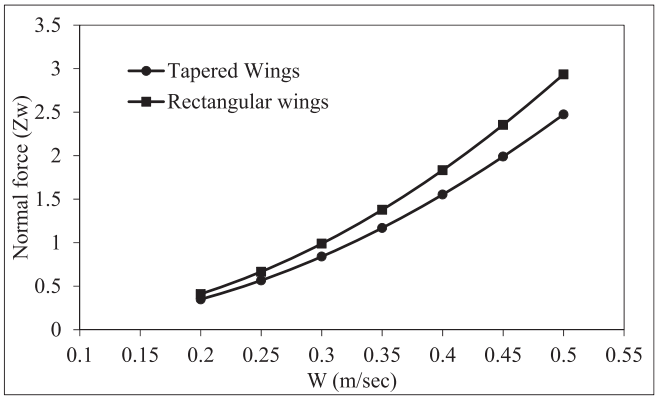


Fig. 16. Variation of normal force ($Z_w$) and heave velocity (W).

*4.7.2. Rotary arm test*

For evaluating stability, rotary hydrodynamic derivatives such as normal force and moment force at various angular velocities are required. The rotary derivatives of the glider can be determined by rotating the flow around the glider, using rotating arms at various angular velocities. Fig. 18 illustrates the flow scheme of fluid around the glider model along the X and Z plane, whereby a flow field is created around the glider with a certain radius (R) to achieve the required angular velocity. Fig. 4 shows the rotating domain

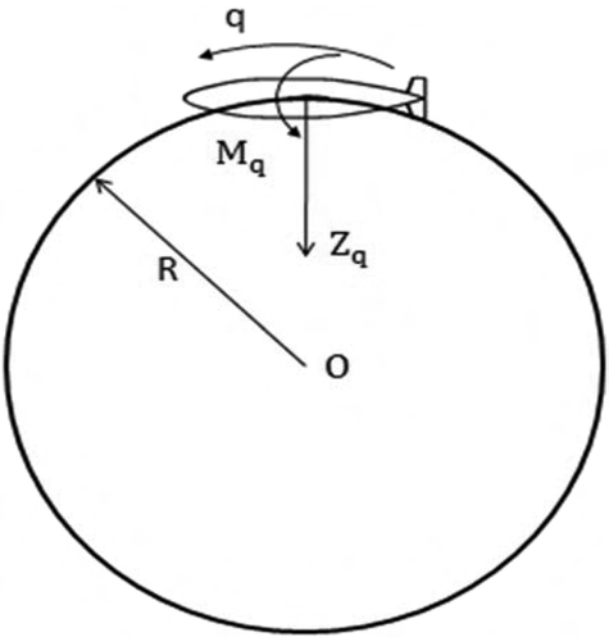


Fig. 18. Force and moment component versus angular speed.

of the fluid around the glider with a radius of 13 m. The angular velocity of the fluid was varied from 0.195 rad/s to 0.52 rad/s, with increments of 0.065 rad/s in angular velocity. The glider model was kept at the constant radius, R to achieve various angular velocities against linear velocity, U. Normal heave force, $Z_q$ and pitch moment, $M_q$ are determined from the slope of the heave force, Z and pitch moment, M with velocity as shown in Figs. 19 and 20.

*4.7.3. Dynamic stability*

Table 4 shows the values of the hydrodynamic derivatives of the UTP glider, which was determined from the numerical simulation, by taking the gradient of the plots of normal forces and moments. The dynamic stability of the glider with rectangular and tapered wings was determined using equation (6) based on the numerical derivatives from Table 4. The studies showed that the vertical dynamic stability margin is 0.93438 and 0.92389 for the glider with tapered and rectangular wings respectively.

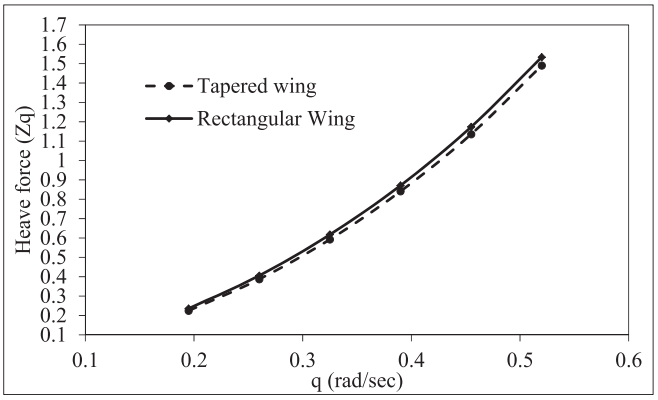


Fig. 19. Rotating heave force, $Z_q$ versus angular velocity (q).

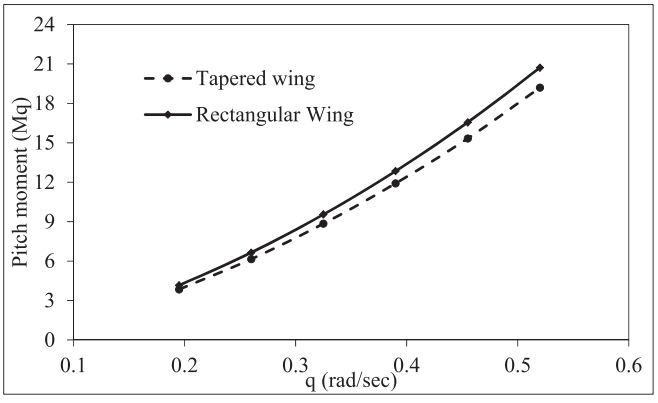


Fig. 20. Rotating pitch moment, $M_q$ versus angular velocity (q).

Table 4
Hydrodynamic derivatives of the UTP glider.

| Derivatives | Tapered Wings | Rectangular wings |
|---|---|---|
| $M_w$ | 1.342 | 1.9586 |
| $Z_w$ | 7.0852 | 8.4154 |
| $Z_q$ | 47.909 | 56.256 |
| $M_q$ | 31.2532 | 32.571 |

## 5. Conclusion

In this study, the effect of wing form on the hydrodynamic characteristic and dynamic stability of an underwater glider was examined, based on numerical and experimental results. These results could be helpful for new design for better maneuverability and control surface for underwater glider to similar shape glider with wings and operational conditions. The numerical simulation shows good agreement with the tow tank experimental results. In summary;

1 The glider with tapered wings form has the positive relation between the velocities of the glider at same glider angle as compared to the rectangular wing.
2 The glider with rectangle wings has better dynamic stability with higher lift force due to larger wetted area, which counteracts the roll moment.
3 Lung capacity factor has a positive correlation with the glider velocity, as it reduces the drag force.

## Acknowledgment

The authors are thankful to Universiti Teknologi PETRONAS for providing the resources required for this work.

## References

Bertin, J.J., Smith, M.L., 1998. Aerodynamics for Engineers.
Bertram, V., 2011. Practical Ship Hydrodynamics. Elsevier.
Fossen, T.I., 2011. Handbook of Marine Craft Hydrodynamics and Motion Control. Wiley.
Graver, J.G., 2005. Underwater Gliders: Dynamics, Control and Design. Citeseer.
Jagadeesh, P., Murali, K., Idichandy, V., 2009. Experimental investigation of hydrodynamic force coefficients over AUV hull form. Ocean. Eng. 36, 113–118.
Javaid, Muhammad Yasar, Ovinis, Mark, Thirumalaiswamy, Nagarajan, Hashim, Fakhruldin B.M., Maimun, Adi, Ullah, Barkat, 2015. Dynamic motion analysis of a newly developed autonomous underwater glider with rectangular and tapered wing. Indian J. Geo-Marine Sci. 44 (12), 1928–1936.
Javaid Muhammad Yasar, O.M., Nagarajan, T., Ali, Syed Saad Azhar, Ullah, Barkat, 2015. Study on wing aspect ratio on the performance of a gliding robotic fish. Appl. Mech. Mater. 789, 248–253.
Liu, F., Wang, Y., Niu, W., Ma, Z., Liu, Y., 2014. Hydrodynamic performance analysis and experiments of a hybrid underwater glider with different layout of wings. In: Oceans 2014-Taipei, pp. 1–5.
Phillips, A.B., 2010. Simulations of a Self Propelled Autonomous Underwater Vehicle. University of Southampton.
Stern, F., Yang, J., Wang, Z., Sadat-Hosseini, H., Mousaviraad, M., Bhushan, S., et al., 2013. Computational ship hydrodynamics: nowadays and way forward. Int. Shipbuild. Prog. 60.
Zhang, S., Yu, J., Zhang, A., Zhang, F., 2013. Spiraling motion of underwater gliders: modeling, analysis, and experimental results. Ocean. Eng. 60, 1–13.
Zhang, F., Thon, J., Thon, C., Tan, X., 2014. Miniature Underwater Glider: Design and Experimental Results.